8-2014

Thick Target Yield of Th-229 via Low Energy Proton Bombardment of Th-232

Justin Reed Griswold
University of Tennessee - Knoxville, jgriswo1@utk.edu

To the Graduate Council:

I am submitting herewith a thesis written by Justin Reed Griswold entitled "Thick Target Yield of Th-229 via Low Energy Proton Bombardment of Th-232." I have examined the final electronic copy of this thesis for form and content and recommend that it be accepted in partial fulfillment of the requirements for the degree of Master of Science, with a major in Nuclear Engineering.

Lawrence H. Heilbronn, Major Professor

We have read this thesis and recommend its acceptance:

Howard L. Hall, Laurence F. Miller

Accepted for the Council:
Dixie L. Thompson

Vice Provost and Dean of the Graduate School

(Original signatures are on file with official student records.)

Thick Target Yield of Th-229 via Low Energy Proton Bombardment of Th-232

A Thesis Presented for the
Master of Science
Degree
The University of Tennessee, Knoxville

Justin Reed Griswold
August 2014

Dedication

To my parents, Joel and Jackie Griswold, and my sister Jessica Griswold. This would not have been possible without all of your love and unwavering support, and for that I dearly thank you.

Acknowledgements

Thank you to Dr. Saed Mirzadeh at Oak Ridge National Laboratory for his inspiration on this project as well as his countless hours of work spent guiding me through the research. Also thank you to Dr. Lawrence Heilbronn for his guidance and leading me towards my academic achievements at the University of Tennessee Department of Nuclear Engineering.

Abstract

Actinium-225 is one of the more effective radioisotopes used in alpha radioimmunotherapy. Due to its ten-day half-life, it is more efficient to create its precursor, ^{229}Th [Thorium-229] ($t_{1/2}$[half-life] = 7932 ± 55 years). In this work, ^{229}Th was produced via 40 MeV [Mega electron Volts] proton bombardment of a thick ^{232}Th [Thorium-232] target. The irradiation took place at the Holifield Radioactive Ion Beam Facility (HRIBF) at Oak Ridge National Lab (ORNL). The target, consisting of 23 stacked natural thorium foils (137 mg/cm^2 [milligrams per square centimeter] each), was irradiated with 50 nA [nanoamps] of protons from HRIBF's 25 MV [Mega Volt] tandem electrostatic accelerator for approximately 143 discontinuous hours. After 215 days post bombardment, allowing for the decay of short-lived protactinium and actinium isotopes and fission products, the target was chemically purified by a series of ion chromatography techniques. Thorium-229 was measured directly by γ-ray [gamma-ray] spectroscopy immediately after separation of the thorium fraction from the decay daughters of ^{228}Th [Thorium-228] ($t_{1/2}$ = 1.9 years) and long long-lived fission products. The effective thick target cross section of ^{229}Th is 205 ± 18 mb [millibarns] at a proton energy of 26.1 MeV. Variation of the effective cross-section as a function of proton energy is also reported.

Table of Contents

List of Tables

List of Figures

Chapter I Introduction and General Information

1.1 Targeted-Alpha Radioimmunotherapy

Radioimmunotherapy using α-emitting radionuclides is currently one of the most promising and rapidly expanding methods for treating oncologic diseases. In recent years, it has been shown that transporting the α-emitting radionuclides by biological carriers such as engineered peptides and antibodies to precise locations of tumor tissues or metastatic cells results in selective irradiation of targeted tissues with minimal damage to normal and non-target tissues.[1] This is due to the fact that the high initial energy of α-particles and their short range in biological tissues allow deposition of high energy in the vicinity of decaying radionuclides.[1] Typical α-particles are emitted from radionuclides with an energy of 5-8 MeV and a range of about 100 microns in tissue; about the same distance as ten cell diameters. Consequently, α-emitters are most suitable for the treatment of micro metastases and have shown to be very effective in treatment of blood cancers such as acute myeloid leukemia (AML), and appear promising in the treatment of micro-metastases in neoplastic diseases.[2, 3, 4] Of the approximately one million new cases of cancer (excluding non-melanoma skin cancer) that occur annually in the United States, about 33% already have metastases, with the remaining initially appearing as local disease. About 40% of these will subsequently develop distant metastases.[5] This particular subset of patients with micro-metastases may benefit from adjuvant α-therapy. Recent clinical trials have shown that relapsed cancer patients who have not responded to conventional chemotherapy can be treated using radiolabeled antibodies with extraordinary success.[6] The potential applications of α-emitters in treatment of other malignancies, such as melanomas, breast, prostate and lung cancers have also been demonstrated.[7, 8, 9, 10]

Of the prospective α-emitters, ^{212}Bi ($t_{1/2}$ = 60 min), ^{223}Ra ($t_{1/2}$ = 11.4 d), ^{225}Ac ($t_{1/2}$ = 10.0 d), and ^{211}At ($t_{1/2}$ = 7.2 h) are of major interest.[11, 12] However, considering the combined nuclear, physical, chemical and biological properties, ^{225}Ac and its daughter ^{213}Bi ($t_{1/2}$ = 45.6 min) are of the most interest.[12, 13, 14] Ongoing clinical trials with ^{213}Bi have demonstrated its efficacy in treatment of oncologic diseases. It is particularly important that ^{213}Bi can be used at early stages of treatment of practically all cancer types, as well as in combination with other methods such as surgery and chemotherapy.[15] A recent review of the target alpha therapy is available.[16]

1.2 Current Supply and Production of ^{229}Th

Bismuth-213 and its precursor, ^{225}Ac are the decay products of long-lived ^{229}Th ($t_{1/2}$ = 7932 ± 55 y). In turn, ^{229}Th is a decay product of ^{233}U, and can be obtained from old stockpiles of this very long-lived isotope of uranium.[17, 18] Figure 1 illustrates the decay process, starting with ^{233}U from which ^{229}Th is currently produced, and continuing through two generator systems involving four intermediate radioisotopes and finally resulting in ^{213}Bi, with a half-life of 45.6 minutes. Current availability of ^{225}Ac/^{213}Bi is insufficient to support existing clinical trials and laboratory investigations. Additionally, new clinical trials are not being initiated since patients could not benefit from any applications developed due to the lack of sufficient quantities of ^{225}Ac/^{213}Bi.

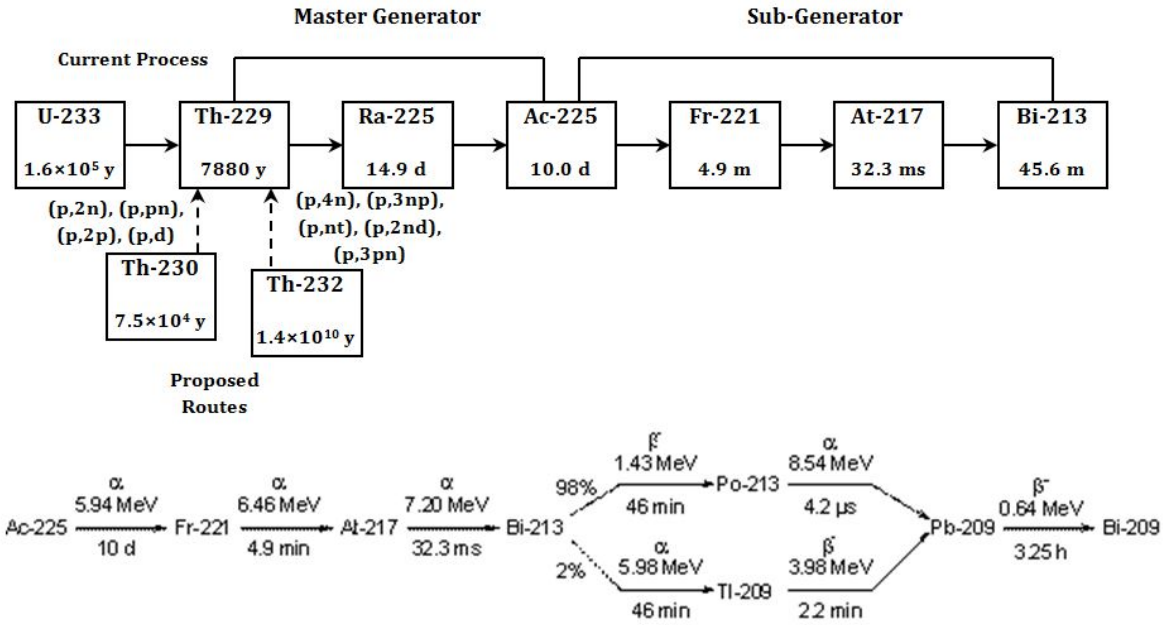

Figure 1. ^{233}U Decay Chain/^{229}Th-^{225}Ac-^{213}Bi Generator Systems

A number of methods are currently being pursued for producing useful quantities of ^{229}Th, and ^{225}Ac:

a. extraction of ^{229}Th from existing ^{233}U stockpiles[17],

b. production of ^{229}Th by multiple and single neutron capture of ^{226}Ra and ^{228}Ra targets in a high flux nuclear reactor, ^{226}Ra[3n,2β]^{229}Th and ^{228}Ra[n,β]^{229}Th reactions,[18]

c. ^{225}Ac can be made directly utilizing the ^{226}Ra[p,2n] or ^{226}Ra[γ,n] ^{225}Ra(15 d , β$^-$) reactions and by spallation reaction of ^{232}Th target with high energy protons.[18, 23]

The current supply of ^{229}Th (extracted from ^{233}U) is insufficient to support multiple clinical trials and the safeguards associated with ^{233}U limits access to this valuable source.[18] The production of

^{229}Th via neutron irradiation of a ^{226}Ra target in a nuclear reactor, ^{226}Ra[3n,2β]^{229}Th reaction, yields about 1000 fold greater activity levels of ^{228}Th ($t_{1/2}$ = 1.8 y) than ^{229}Th, and the 2.6 MeV γ-ray in the ^{228}Th decay chain poses shielding problems for large-scale production via this route. [18]

The required fast turn-around for processing the Ra target in the direct production of ^{225}Ra and ^{225}Ac (a few days post-irradiation) is the main disadvantage for proton and γ-ray irradiation of a ^{226}Ra target, and proton spallation of ^{232}Th target. Continuous processing of radium targets for the direct production of ^{225}Ra and ^{225}Ac is far more challenging than routine extraction of ^{225}Ra and ^{225}Ac from the long-lived ^{229}Th. Further, simultaneous production of rather large quantities of fission products in the high energy (E_p >100 MeV) proton-irradiated ^{232}Th target is an additional complexity associated with this approach. Thus, developing a stockpile of ^{229}Th may prove to be the best means of providing ^{225}Ra and ^{225}Ac in the long run.

As an alternative to the production methods currently being pursued, ^{229}Th can be produced by low energy proton bombardment of ^{232}Th targets. Among possible reactions the [p,4n] reaction on a ^{232}Th target is of main interest in proton energies below 50 MeV. This reaction yields ^{229}Pa which decays via *EC* process (99.5%) with a $t_{1/2}$ of 1.5 d to ^{229}Th. It is important to note the 0.5% of the time, the α-decay of ^{229}Pa directly feeds into ^{225}Ac.[25] At somewhat higher energies, the contribution of the ^{232}Th[p,α]^{229}Ac ($t_{1/2}$ = 62.7 min, β^-) ^{229}Th reaction to the overall yield of ^{229}Th cannot be ignored. A summary of the threshold energies and coulombs barriers for possible reactions leading to the formation of ^{229}Th in proton bombardment ($E_p \leq 40$ MeV) of ^{232}Th targets is given in Table 1. Figures 2 and 3 are graphic representations of the chart of the nuclides that facilitate interpretation of the various reactions leading to the formation of ^{229}Th from ^{230}Th and ^{232}Th.

Table 1. ^{229}Th Production Reactions (NNDC, 2009). Threshold energies were calculated from systematics using nuclide masses and conservation of momentum (NNDC, 2009).

Target /Reaction	Threshold (MeV)	Exit Coulomb Barrier (MeV)
^{232}Th	**Entrance Coulomb Barrier = 12.1**	
^{232}Th(p,nt)^{229}Th	9.9	14.1
^{232}Th(p,2nd)^{229}Th	16.2	14.1
^{232}Th(p,3np)^{229}Th	18.4	14.1
^{232}Th(p,4n)^{229}Pa(EC, $t_{1/2}$ = 1.5 d)^{229}Th	19.5	0
^{232}Th(p,α)^{229}Ac(β, $t_{1/2}$ = 1.0 h)^{229}Th	0	27.9
^{232}Th(p,pt)^{229}Ac(β, $t_{1/2}$ = 1.0 h)^{229}Th	10.3	27.9
^{232}Th(p,n^{3}He)^{229}Ac(β, $t_{1/2}$ = 1.0 h)^{229}Th	11.1	27.9
^{232}Th(p,2d)^{229}Ac(β, $t_{1/2}$ = 1.0 h)^{229}Th	14.3	27.9
^{232}Th(p,npd)^{229}Ac(β, $t_{1/2}$ = 1.0 h)^{229}Th	16.6	27.9
^{232}Th(p,2n2p)^{229}Ac(β, $t_{1/2}$ = 1.0 h)^{229}Th	18.8	27.9
^{232}Th(p,p^{3}He)^{229}Ra(β, $t_{1/2}$ = 4.0 m)^{229}Ac(β, $t_{1/2}$ = 1.0 h)^{229}Th	12.1	41.4
^{232}Th(p,2pd)^{229}Ra(β, $t_{1/2}$ = 4.0 m)^{229}Ac(β, $t_{1/2}$ = 1.0 h)^{229}Th	17.6	41.4
^{232}Th(p,3pn)^{229}Ra(β, $t_{1/2}$ = 4.0 m)^{229}Ac(β, $t_{1/2}$ = 1.0 h)^{229}Th	19.8	41.4

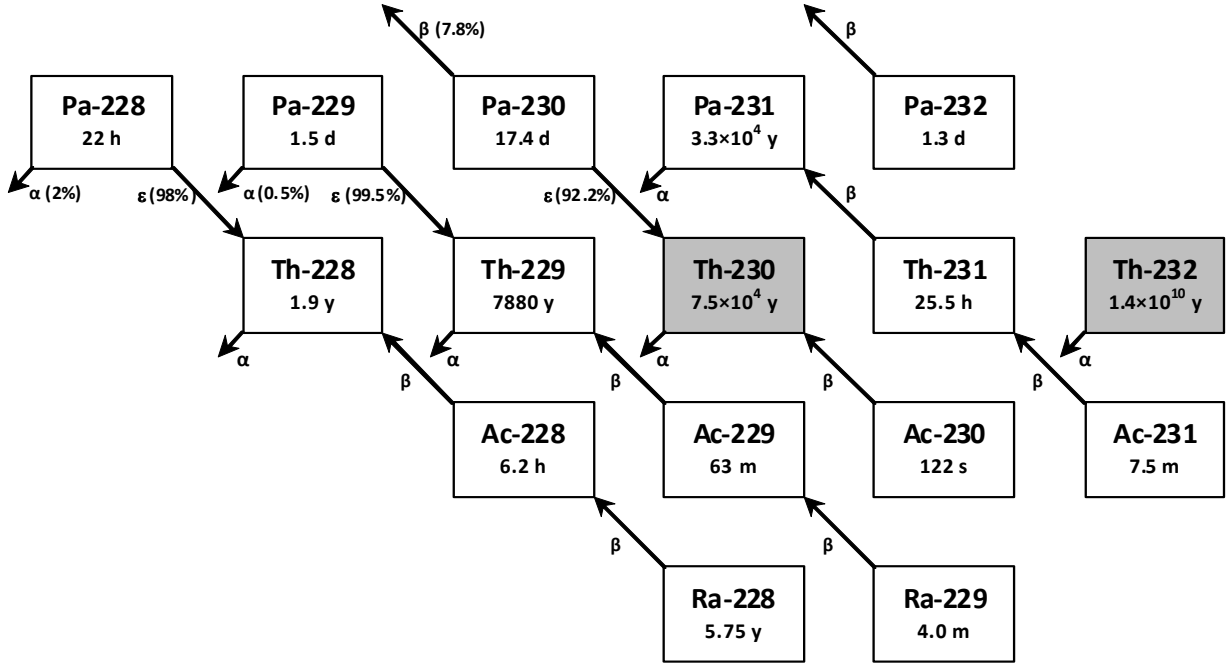

Figure 2.Thorium Production Nuclides Decay Scheme

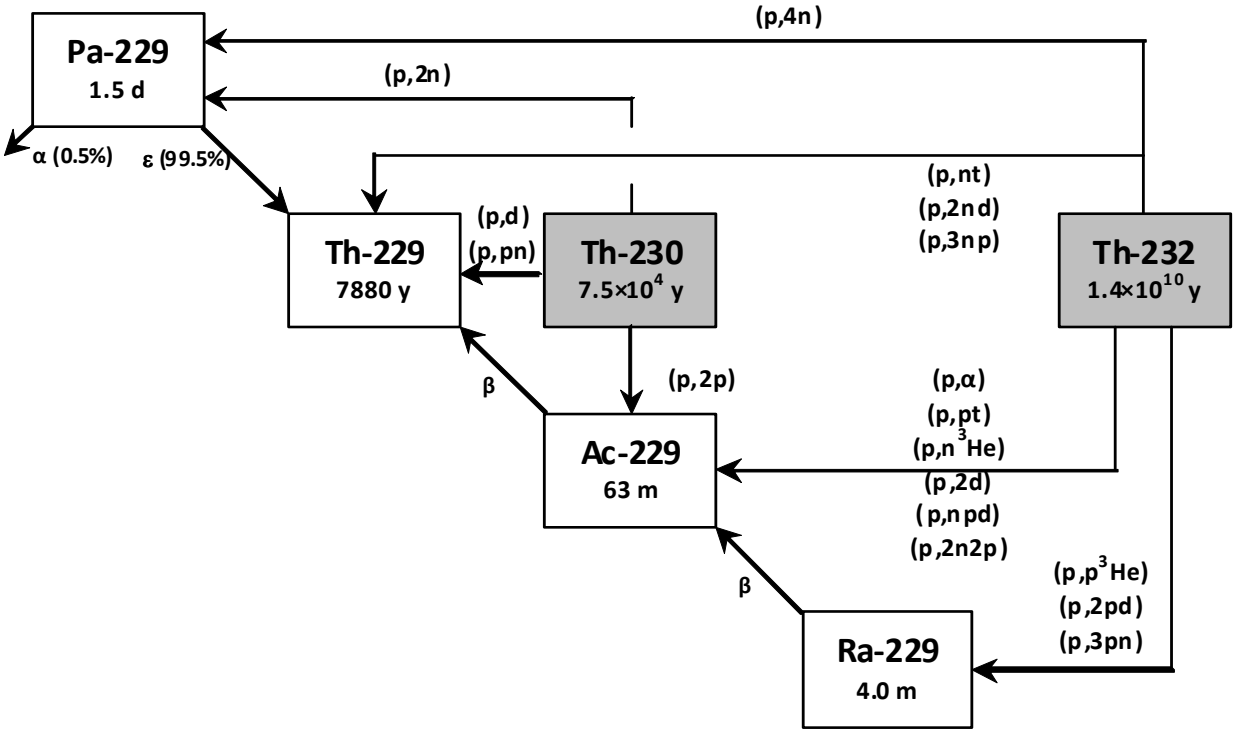

Figure 3. Thorium Proton Bombardment Reaction Block Diagram

Several experiments have been conducted bombarding low energy protons (10-40 MeV) on a natural thorium foil target. The measured cross-sections for proton induced reactions on natural Th yielding to $^{228, 229, 230 \& 232}$Pa isotopes (^{232}Th[p,xn] reactions, where x = 1, 3, 4, and 5) have been reported and are shown in Figure 4[26]. Natural thorium was deposited onto high purity aluminum foil using sputter deposition for the measurement of the ^{232}Th[p,3n]^{230}Pa reaction.[19]

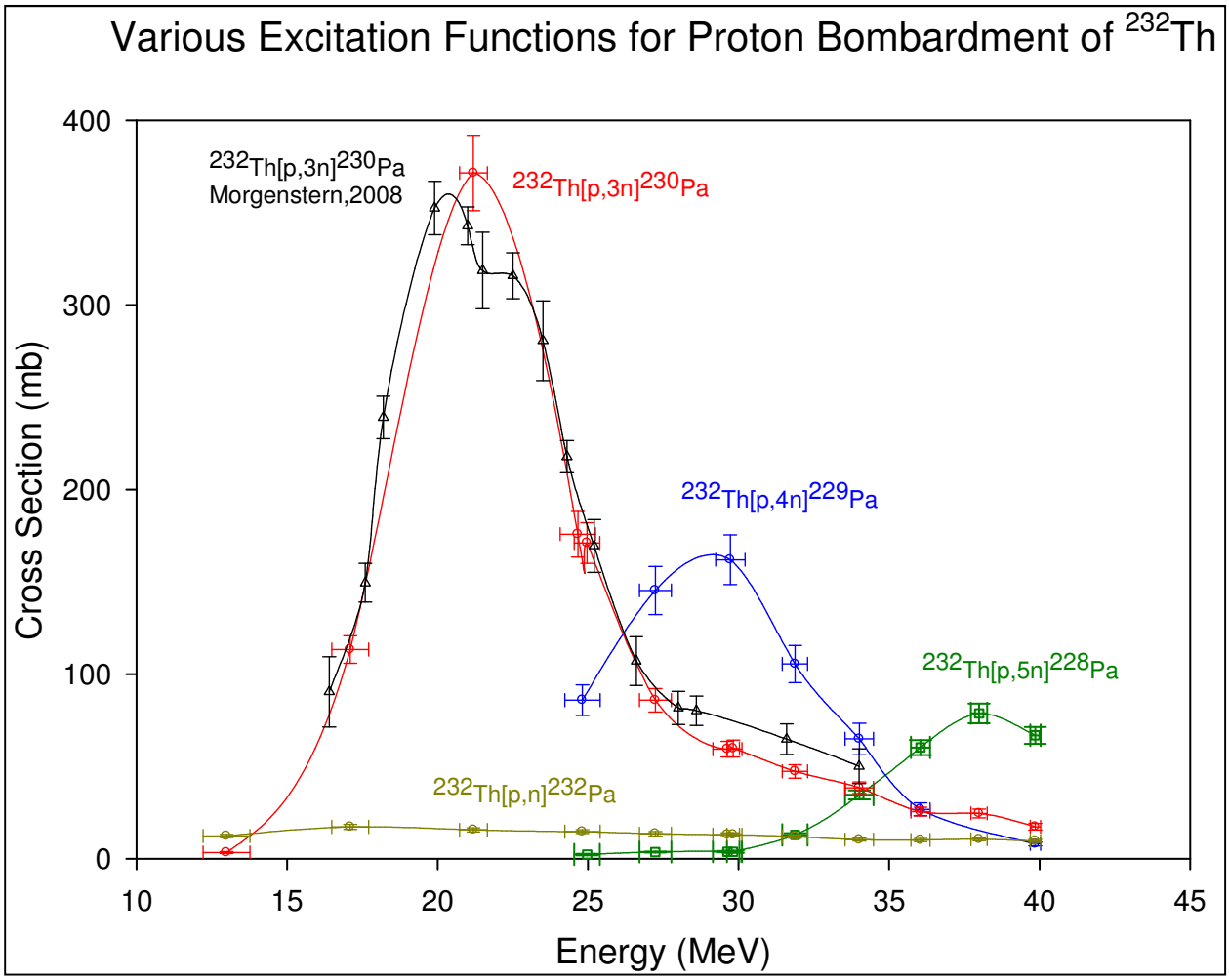

Figure 4. Previously measured ^{232}Th[p,xn] excitation functions

Chapter II Objective and Theory

This thesis focuses on the production of ^{229}Th via low energy proton bombardment of a thick natural thorium target. The main goal is to prove viability of this method of production to supplement the current supply of ^{229}Th that is used as a sustainable source of ^{225}Ac. The effective thick target cross section for the ^{232}Th[p,x]^{229}Th reaction is reported for the first time. Radioactivity of ^{229}Th was determined post-irradiation by γ-ray spectroscopy of emissions specific to the nucleus of ^{229}Th. This is significant due to the very long half-life of ^{229}Th and the subsequently low amount of activity produced (nanoCi quantities). Because of this relatively low activity level, radiochemical purification of the thorium targets post-irradiation was essential. Specific contributions to the experiment include pre-irradiation target design, target fabrication, post-irradiation radioactivity assay, post-irradiation chemical purification, and activity and cross section analysis. Assembling the irradiation set-up as well as obtaining the irradiation data were performed by Dan Stracener and Carola Jost of the ORNL Physics Division. The design and fabrication of the aluminum target holder which is described in further detail in Chapter 2 was conducted by David Denton from the ORNL Medical Radioisotope Program.

2.1 Heavy Charged Particle Interactions in Matter

Heavy charged particles are considered to be any charged particle other than an electron or a positron. When traveling through matter, these particles mostly lose energy through the ionization and excitation of atoms. These particles interact with atomic electrons via the Coulomb force, transferring small fractions of their incident energy in each collision. Interactions with atomic nuclei can occur, but are rare in comparison to collisions with electrons. A useful quantity relating the energy lost by heavy charged particles in matter is stopping power (MeV/cm). The Bethe formula for stopping power is given in the equation below where k_0 is a

constant, z is the atomic number of the heavy particle, e is the magnitude of the electron charge, n is the number of electrons per unit volume in the medium, m is electron rest mass, c is the speed of light in a vacuum, β is the speed of the particle relative to c (V/c), and I is the mean excitation energy of the medium.[20]

$$-\frac{dE}{dx} = \frac{4\pi k_0^2 z^2 e^4 n}{mc^2\beta^2}\left[ln\frac{2mc^2\beta^2}{I(1-\beta^2)} - \beta^2\right]$$

This value can be divided by the density to give mass stopping power. Range of a heavy charged particle is very small relative to electrons or neutrons of the same energy and is given by the integral of the inverse stopping power.

$$R(T) = \int_0^T \left(-\frac{dE}{dx}\right)^{-1}$$

When considering a beam of heavy charged particles, it is important to note the effects of energy straggling and multiple scattering. Energy straggling is the fluctuation of charged particle energy in a beam of particles due to the random nature of electronic collisions. Each heavy charged particle will travel in a similar but not identical path through a target material, allowing for a small variance in incident particle energy as the beam travels through the material. Multiple scattering is a series of collisions that cause significant deviations from the incident heavy charged particle direction. This causes a monoenergetic beam of particles to diverge as it traverses through an absorber, which, in turn leads to a distribution of particle energies at a specific depth in the material.

Chapter III Materials and Methodology

3.1 Materials and Equipment

Natural thorium foils, (99.9%, ~0.0125 and 0.125 mm in thickness) were obtained from Goodfellow Corporation (Ermine Business Park, 7 Spitfire Close, Huntingdon PE29 6WR, United Kingdom). High purity (99.45%) Al foils (0.025 mm thick) used as cover foils were obtained from Alfa Aesar, (26 Parkridge Rd. Ward Hill, MA 01835).

The ion exchange resins MP1 (Cl^- form, 200-400 mesh), and disposable polypropylene (PP) columns [2 mL bed volume (BV) and a 0.8 cm I.D.] were purchased from Bio-Rad Laboratories (4000 Alfred Nobel Drive Hercules, CA 94547), and resins were stored in deionized water. As needed the MP1 resin in chloride form was converted to nitrate form by washing the resin with 4 BV of 8 M HNO_3, followed by 4 BV of deionized water. The nitrate converted resin was always stored in deionized water. Three separate columns were used for this experiment. Column A was a 0.4 mL MP1/Cl^- pre-equilibrated with 1 mL of 10 M HCl before use, Column B was a 3 mL BV MP1/NO_3^- which was pre-equilibrated with 8 M HNO_3 before use, and column C was same as column B except with a 0.4 mL BV.

A liquid nitrogen cooled High Purity Intrinsic Germanium (HPGe) detector was used for all radioactivity measurements conducted throughout the course of this experiment. More information regarding details about detector geometry, efficiency, and resolution can be found in Section 3.4.

3.2 Target Assembly and Irradiation

3.2.1 Target Assembly and Geometry

The natural thorium foil target was constructed using the stacked foil technique. Originally arriving as one 0.125mm thick, 50 mm x 50 mm sheet from the Goodfellow Corporation, the sheet was carefully cut into 25 10 mm x 10 mm square foils. Since this experiment did not call for the proton beam to be stopped within the target, a simple proton energy degradation calculation was performed to determine the number of foils needed to degrade the proton beam energy below 10 MeV but not allow a significant number of the protons to be absorbed. The details of this calculation are shown in Section 3.2.3. It was determined that 23 foils would allow for an exit energy of 12 MeV. Twenty-three 0.125 mm (137 mg/cm^2 each) natural thorium foils were stacked on top of each other for a total areal density of 3.15 g/cm^2. Two 0.025 mm high purity aluminum foil disks were used as cover foils. A photograph of one of the foils pre-irradiation is displayed in Figure 5. An aluminum target holder, Figure 6 and Figure 7, was created to house the target foils.

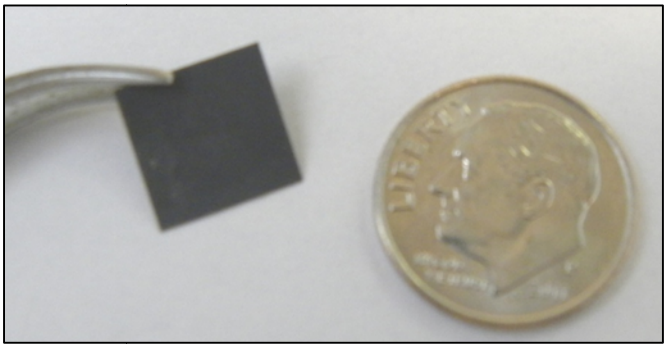

Figure 5. Picture of one of the 10mm x 10mm square foils next to a coin for scale.

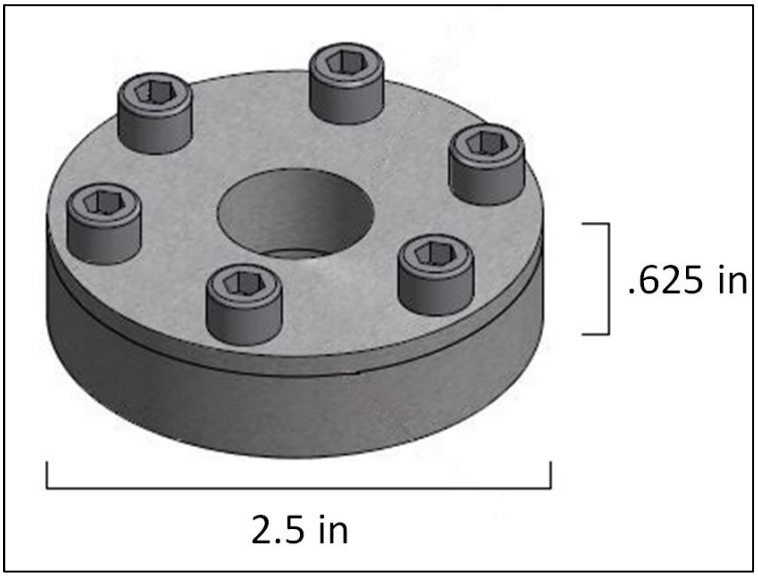

Figure 6. Scaled drawing of aluminum target holder

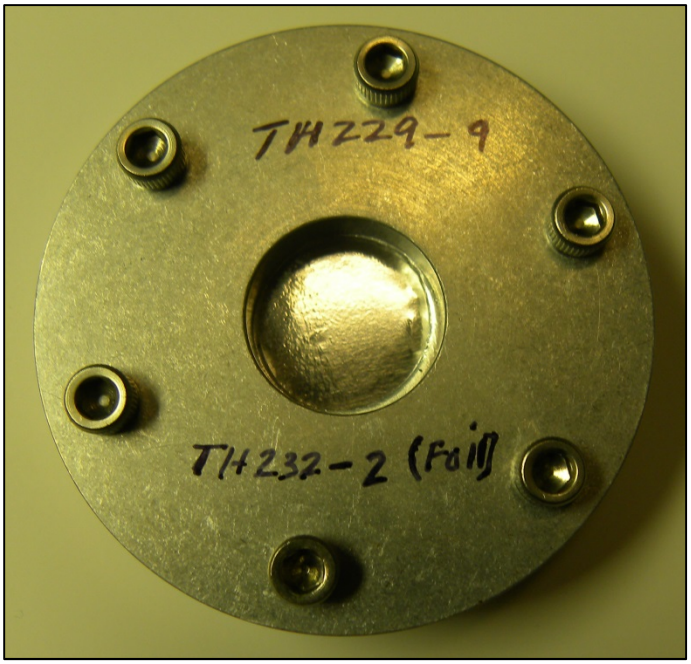

Figure 7. Packaged aluminum target holder with thorium foils inside.

3.2.2 Irradiation Details

The irradiation took place at the On-Line Test Facility (OLTF), a low intensity Isotope Separation On-Line (ISOL) facility primarily used for testing of ion sources and targets for the production of radioactive ion beams located at ORNL's Holifield Radioactive Ion Beam Facility (HRIBF) [Carter and Stracener 2008]. Proton beams of up to 40 MeV in energy and 50 nA of intensity can be delivered from the Tandem accelerator.[21]

For the cross section measurements, the target was stacked in the Al holder (Figure 7) which was mounted in a Cu fixture in a standard HRIBF target-ion source enclosure (Figure 8). A Faraday cup was positioned directly behind the target for continuous monitoring of the proton beam during irradiation. The Cu mounting fixture is connected to a water-cooled Cu feed-through to provide target cooling, but for this experiment water cooling was not required. The Tandem beamline connecting to the enclosure contains diagnostics to measure the size, position, and intensity of the beam just before entering the target. The proton beam scatters in the thick target, and only a fraction of the beam is observed in the Faraday cup after the target. This fraction depends on beam energy and thickness of the target. Periodic measurements of the beam currents before and after the target allow for a determination of the fraction of beam observed in the Faraday cup after the target. This ratio coupled with the continuous measurement of the current after the target provides for a precise calculation of the number of protons hitting the target. Two independent methods were used to determine the incident proton energy at each foil and are discussed in Section 3.2.3.

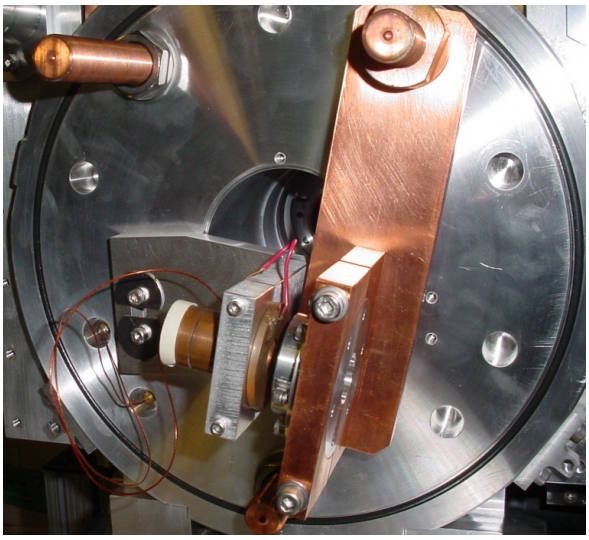

Figure 8. Target assembly at HRIBF with the Faraday cup located on the left-hand side of the target and the beam entering from the right.

Since the main goal of this irradiation was to create the long-lived ^{229}Th, a longer irradiation period was required. However, due to the busy schedule of the Tandem accelerator at HRIBF, a long, continuous irradiation was not feasible. Therefore the irradiation took place over five discontinuous stages lasting from 13 to 38 hours and accumulating a total of over 143 hours of beam time over a span of about 44 days. For this experiment, 40 MeV proton beams were used with an average current of 47 nA and the total accumulated charge was 6.72 μA-hrs.

3.2.3 Degradation of Proton Energy Through Target Stack

In order to develop a comprehensive excitation function throughout the desired energy range (10-40 MeV), calculations were necessary to determine the total number of foils required as well as the overall areal density of the target package. The first of two independent calculations of the proton energy throughout the proposed target package was a simple spreadsheet using NIST stopping power tables to "step through" each foil.[24] Mass stopping power was given (in MeV*cm^2/g) for each incident proton energy and then multiplied by the

areal density (in g/cm^2) of thorium to give the energy loss (in MeV) of the incident protons. In some cases interpolation was used to calculate the stopping power of an incident proton that was in between two given energy values. This method provides a rough estimate of incident proton energy at the surface of each foil, but fails to account for phenomena such as range straggling and multiple scattering.

The second method to determine the energy loss throughout the target package used the computer code TRIM (transport of ions in matter). TRIM is a Monte Carlo based code that follows a user-specified (usually very large) number of particle histories in a user-created target. As implied by the name, TRIM only models the transport of heavy charged particles and is not applicable to the transport of γ-rays, electrons, positrons, or neutrons. Particle energy is lost through nuclear or electronic collisions, and the particle history ends when the particle reaches a minimum energy or is scattered outside of the target. The applicable range of ion energies is from 0.1 keV/u to "several" MeV/u.[22] When compared to other programs utilizing the Monte Carlo technique, one of the main advantages TRIM provides is the ability to cut down computing time by up to 50x over other programs. However, with this increased speed, some assumptions must be made such as neglecting nuclear reactions, relativistic effects, and directional properties of the crystal lattice of the target material.

A comparison of the two methods for calculating proton energy degradation is shown below in Figure 9. Although the first method using the stopping power tables was originally used as a rough estimate, the final energy values used in this thesis were obtained from TRIM and are displayed in Table 2. It is important to note that the TRIM calculation gives a lower energy at each foil; this is due to the inclusion of important factors such as range straggling and multiple scattering. Error bars are included for the TRIM points but are too small to be visible.

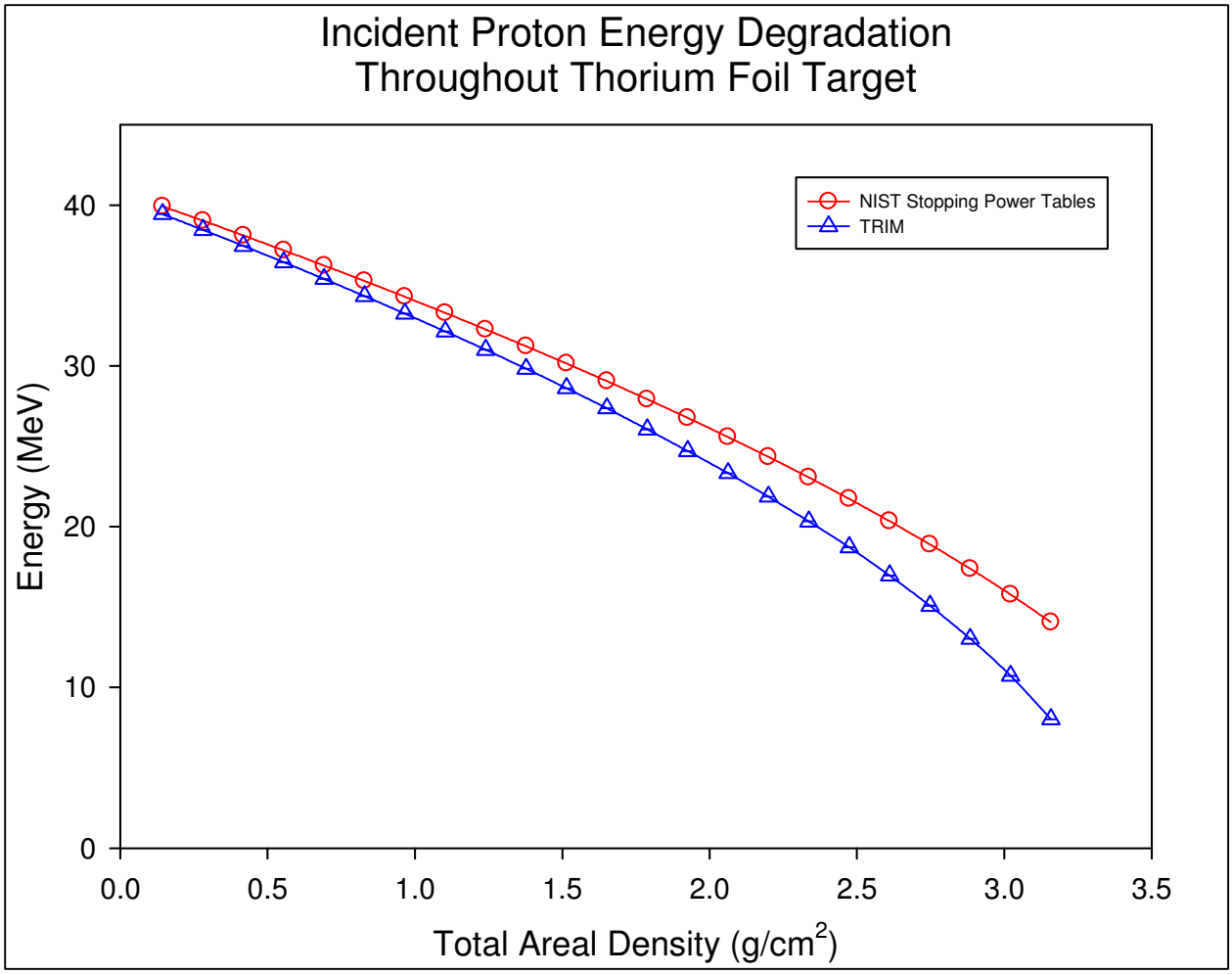

Figure 9. Comparison between the two methods used for calculating incident proton energy throughout the thorium foil target package.

Table 2. Average incident proton energy at each foil. Uncertainty increases as energy decreases due to increased range straggling effects at lower energies.

Foil	Total Areal Density (g/cm^2)	Proton Energy (MeV)	Uncertainty
1	0.14	39.44	0.02%
2	0.28	38.46	0.01%
3	0.42	37.46	0.01%
4	0.55	36.45	0.02%
5	0.69	35.41	0.02%
6	0.83	34.34	0.04%
7	0.97	33.25	0.04%
8	1.10	32.14	0.04%
9	1.24	31.00	0.03%
10	1.38	29.83	0.04%
11	1.51	28.61	0.05%
12	1.65	27.37	0.05%
13	1.79	26.05	0.08%
14	1.93	24.70	0.07%
15	2.06	23.33	0.07%
16	2.20	21.86	0.10%
17	2.34	20.33	0.09%
18	2.47	18.72	0.10%
19	2.61	16.97	0.13%
20	2.75	15.08	0.16%
21	2.88	13.03	0.19%
22	3.02	10.72	0.24%
23	3.16	8.02	0.35%

Uncertainty in the mean proton energy was calculated using the following equations where SD is the standard deviation and σ is the standard error :

$$SD = \sqrt{\frac{\sum_{i=1}^{N}(x_i - \bar{x}_N)^2}{N-1}}$$

$$\sigma = \frac{SD}{\sqrt{N}}$$

It is important to note that the uncertainty given is the uncertainty in the mean of proton energies at a specific target depth and not the range of proton energies.

3.3 Post Irradiation Chemical Processing

3.3.1 Dissolution of Thorium Foils

After irradiation, the target consisting of 23 foils was transferred to a chemical hood to prevent contamination, and removed from the aluminum target holder (Figure 7). Then the foils were mounted on individual counting cards and assayed via γ- ray spectroscopy employing a High Purity Germanium (HPGe) detector for 5 hours. The foils were then removed from the counting cards, individually dissolved, and prepared for chemical separation using the following procedure in a standard class-C chemical hood:

1. Carefully placed foil in 20 mL glass scintillation vial using plastic tweezers.
2. Added 2 mL of 10 M HCl. Dissolution began to occur instantly with bubbles appearing in the solution.
3. Added 10 µL of 2 M HF to aid in dissolution. After ~5 minutes, the solution began to become dark and opaque. No boiling or severe bubbling that could cause liquid to escape the vial was allowed to occur.
4. Heated gently using a hot plate around 70-80 °C. The solution became clear after about 1 hour of heating. A small amount of dark blue residue remained at the bottom of the vial.
5. In order to separate the target solution from the remaining dissoluble solids, the mixture needed to be centrifuged. A glass pipette was used to remove all of the solution, as well as any solids that remained in the vial, and placed in a 5 mL polypropylene centrifuge tube. Rinsed the vial with 1 mL of 10 M HCl and added to the centrifuge tube.
6. Centrifuged for 1 minute.
7. Removed supernatant from remaining residue in centrifuge tube using a clean glass pipette. Placed supernatant into a clean glass scintillation vial.

8. Added 1 mL of 10 M HCl to the centrifuge tube and repeated steps 6 and 7, adding the supernatant to the same clean glass scintillation vial as before.
9. Measured radioactivity in supernatant and remaining residue on HPGe detector for 5 minutes each.
10. Heated supernatant solution to dryness on a hot plate and under a heat lamp. Once the sample was dry, the vial was allowed to cool for 5 minutes.
11. Dissolved the residue in the vial in 0.5 mL 10 M HCl.

3.3.2 Anion Exchange Columns

In order to perform γ-ray spectroscopy on each of the targets, the decay daughters of Th-228 ($t_{1/2}$ = 1.91y) and some of the fission products had to be removed. Anion exchange chromatography was used to separate first the thorium from other the other actinides and fission products. A resin size of 200-400 mesh was used, and the resins were stored in deionized water. Three separate columns were used for each foil: Column A, Column B, and Column C. Figure 10 outlines the chemical process used. Each of the chemical separations was conducted in a standard Class C chemical hood located in a radiochemical laboratory. The method that was used to construct each column was very similar and is outlined below:

1. Marked the desired bed volume (BV) on the side of the column using a permanent marker. Also labeled the column with the date, foil number, and column designation.
2. Wetted the frit of the column using distilled water. Allowed for at least 1 mL of water to pass through the column into a waste collection beaker below.

3. Using a glass pipette, slowly added 200-400 mesh MP1 resin to the column. No resin was dispensed above the desired BV line.
4. Once the desired BV line was reached, rinsed the column above the BV line to make sure that no resin remained above the line.
5. Added a small amount of Pyrex glass wool (about 1 cm tall and at least the width of the column) to make sure resin does not escape. Carefully pressed down glass wool using a glass pipette to make sure wool is snug but not too tight. If the glass wool was pressed down too tight, liquid would not be allowed to flow freely through the wool.
6. Added 4 bed volumes of desired acid to the column (9M HCl if using resin in Cl^- and 10M HNO_3 when converting chloride form resin to nitrate form).
7. Washed with at least 4 bed volumes of distilled water and stored with at least 0.5 mL of distilled water remaining on the column.

3.3.2.1 Column A - MP1 HCl Column

Column A was the first column used and was designed to separate the thorium from fission products such as iron, molybdenum, and niobium as well as from two actinides produced in the irradiation: uranium and protactinium. Some of the other products such as actinium, barium, cesium, lanthanum, and radium remained with the thorium fraction. The column was a BioRad disposable polypropylene (PP) column with a 2 mL available BV and a 0.8 cm bed diameter. The column contained 0.4 mL of the MP1 anion exchange resin in the Cl^- form. The target solution was loaded onto Column A and eluted off of Column A using the procedure below:

1. Conditioned Column A by allowing the distilled water to drip into the waste beaker below the column and adding at least 2 BV of 10 M HCl.
2. Added the target solution to the column using a clean glass pipette. Collected column load in a clean glass scintillation vial labeled “Load/Wash” with the column designation and foil number.
3. Added 0.5 mL 10 M HCl to the now empty target vial to rinse the vial. Pipetted the rinse solution into the column and collected using the same vial as in step 2.
4. Repeated step 3 twice. Once the last 0.5 mL fraction of 10 M HCl was fully collected, assayed the load/wash for 5 minutes on an HPGe detector. This sample should have contained the entire thorium fraction.
5. Added 0.5 mL of either 9M HNO_3, distilled H_2O, or 0.1M HCl to column. This was the “strip” solution. Collected in a clean glass scintillation vial labeled “Strip” with the column designation and foil number. Once the 0.5 mL of solution had dripped entirely into the vial, closed the vial and counted for 5 minutes on an HPGe detector.
6. Heated the load/wash solution to dryness. A hot plate was used at a temperature of 70-80 °C. A heat lamp was also used to decrease the evaporation time. Once the solution dried, allowed the vial cool for 5 minutes prior to adding any liquid.

3.3.2.2 Conversion to Nitrate

In order to complete the next chemical separation, the load solution from column A needed to be converted from a chloride to a nitrate. The process for converting to a nitrate was completed for each foil as follows:

1. Added 1 mL of concentrated HNO_3 to the load solution vial. The liquid in the vial began to turn a faint yellow.

2. Using a hot plate, heated gently at 40-50 °C. Bubbles began to appear as the liquid turned more yellow. After 5-10 minutes of heating the liquid became clear.
3. Once the liquid became clear, heated the solution to dryness. After dryness was achieved, allowed the vial cool before any other liquids were added.
4. Repeated 1-3. The yellow color of the liquid only appeared during the initial dissolution.

3.3.3.3 Column B - First MP1 HNO_3 Column

The second column used, designated column B, separated the thorium fraction from actinium and radium, as well as fission products such as barium, lanthanum, cesium, and lead. Instead of using a PP column, a glass column was used with a 3 mL BV of the same MP1 resin as before. The resin was converted to the nitrate form using 4 BV of HNO_3 during the column construction process. Column B was processed using a similar method but not exactly like column A:

1. Conditioned the column by allowing the distilled water to drip into the waste beaker below the column and adding at least 2 BV of 10M HNO_3.
2. Added 1 ml of 10M HNO_3 to dry column A load solution vial. Swirled gently to aid in dissolution of barely visible solids at bottom of vial. Gentle heat (40-50 °C via hot plate) was also added to aid in dissolution.
3. Using a clean glass pipette, transferred the solution to the column. Collected the solution dripping off the column in a clean glass scintillation vial labeled "Load/Wash" along with the column designation and foil number.
4. Repeated steps 2-3 twice, continuing to add the solution from the column into the same vial.

5. Once the final drops of liquid had fallen into the glass scintillation vial, assayed radioactivity in the vial for 5 minutes.
6. Added 3 mL of 0.1M HNO_3 to the column. Collected solution dripping off of column in a clean glass scintillation vial labeled "Strip" with the column designation and foil number. This fraction, designated column strip should contain all or most of the thorium. After the dripping off the column was complete, counted vial for 5 minutes.
7. Evaporated the strip solution to dryness on a hot plate at a temperature of 70-80 °C and under a heat lamp. Once the solution reached dryness, the vial was allowed to cool for 5 minutes before any liquid was added.

3.3.3.4 Column C - Second MP1 HNO_3 Column

Column C was similar in function to column B, but on a smaller scale. Many of the ^{228}Th daughter products were removed in column B, however small fractions of ^{212}Pb ($t_{1/2}$ = 10.64h) pass through the column. Column C was designed in order to remove these products from the thorium fraction, but it is impossible to remove them entirely due to the constant formation of ^{212}Pb from the decay of ^{228}Th. Column C was constructed with a BioRad disposable polypropylene (PP) column with a 2 mL available BV and a 0.8 cm bed diameter. The column contained a 0.5 mL BV of MP1 resin converted to the nitrate form using 2 mL (4 BV) of HNO_3 during column construction. Column C was processed almost exactly like column B with exception of a variation in reagent volumes and the acid used in the strip solution:

1. Conditioned the column by allowing the distilled water to drip into the waste beaker below the column and adding at least 2 BV of 10M HNO_3.

2. Added 0.5 mL of 10M HNO_3 to the dry column B strip solution vial. Swirled gently to aid in dissolution of barely visible solids at bottom of vial. Gentle heat (40-50 °C via hot plate) was also added to aid in dissolution.
3. Using a clean glass pipette, transferred the solution to the column. Collected the solution dripping off the column in a clean glass scintillation vial labeled "Load/Wash" along with the column designation and foil number.
4. Repeated steps 2-3 twice, continuing to add the solution from the column into the same vial.
5. Once the final drops of liquid had fallen into the glass scintillation vial, counted for 5 minutes.
6. Added 0.5 mL of 10M HCL to the column. Collected solution dripping off of column in a clean glass scintillation vial labeled "Strip" with the column designation and foil number. This fraction is designated the strip and should contain all or most of the thorium. This is the final step of chemical purification. Now the sample is ready for assay via γ-ray spectroscopy, which had to be conducted immediately, as ^{212}Pb grew back in very quickly. Details about the γ- ray spectroscopy can be found in the next section.

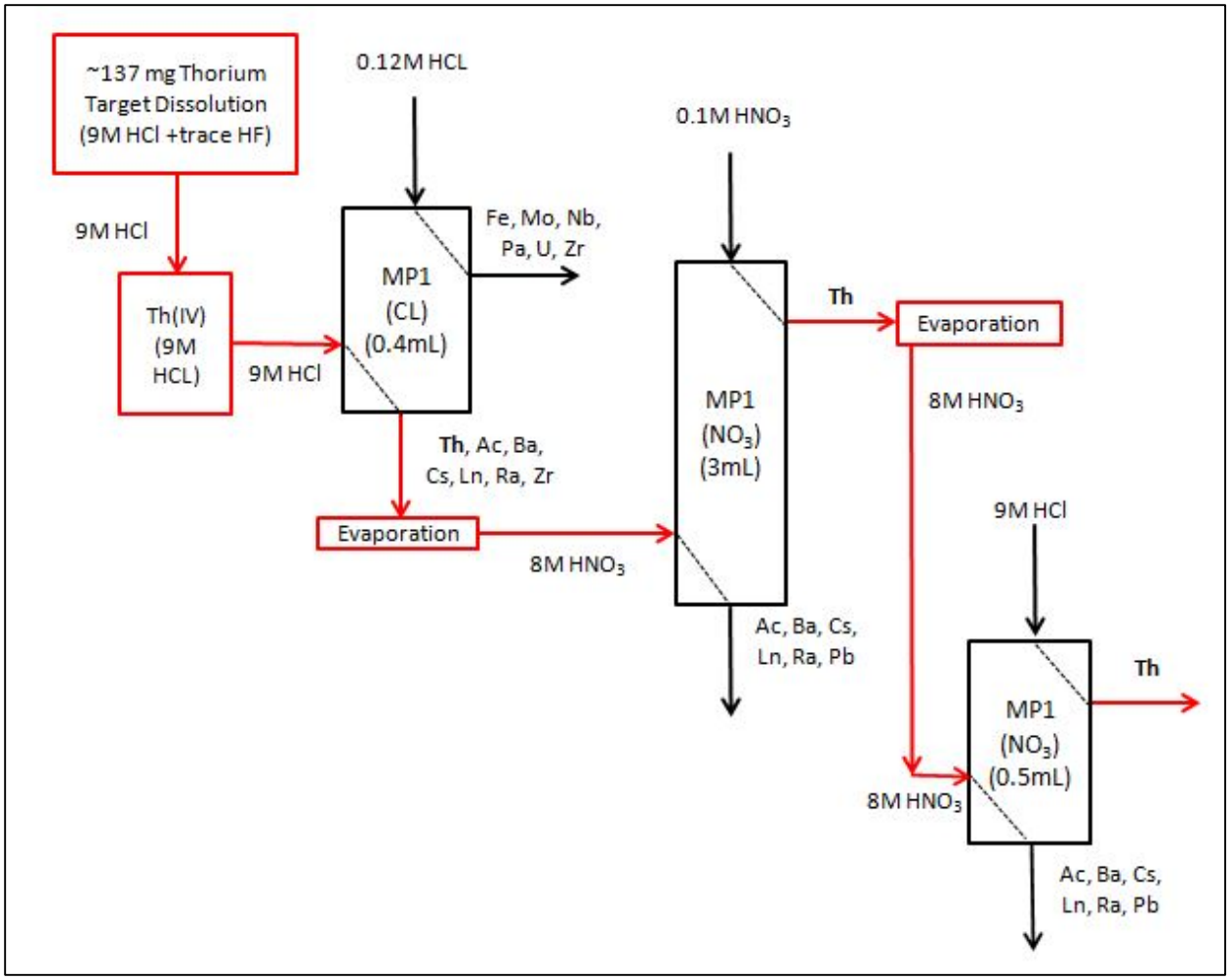

Figure 10. Outline of Chemical Separation Process

3.4 Radioactivity Measurements of Irradiated Foils

The radioactivity measurements for this experiment were conducted using a calibrated HPGe detector. A multichannel analyzer utilizing Canberra Genie 2000 software was coupled to the HPGe detector. According to the manufacturer, the resolution of the detector is 0.74 keV at 122 keV and 2.0 keV at 1332 keV. Energy and efficiency calculations were completed for the detector using a γ-ray source traceable to the National Institute of Standards and Technology (NIST). A typical efficiency calibration is shown in Figure 11. The points are experimentally

measured efficiencies and a solid curve was generated via a 5th order polynomial function. The function of the curve is provided, and the constants for this specific efficiency curve are shown in Table 3. The specific γ-rays and their intensities that were used to assay the radionuclides involved in this work are shown in Table 4.

$$efficiency = \exp(a + b * ln(E) + c * ln(E)^2 + d * ln(E)^3)$$

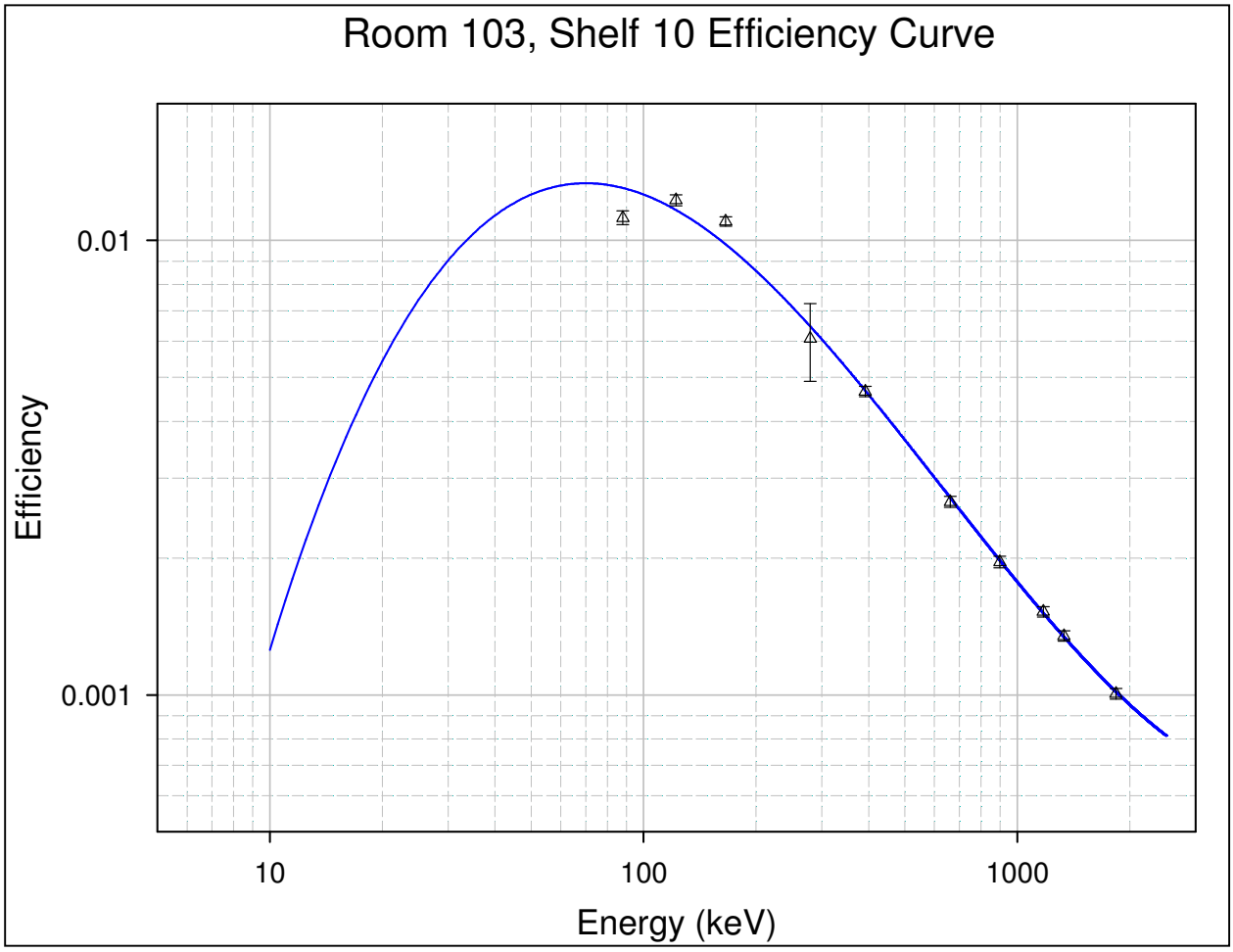

Figure 11. Typical efficiency curve for HPGe detector.

Table 3. Constants used in efficiency function. E is the incident photon energy.

a	b	c	d
-18.628	8.059	-1.415	0.073

Table 4. Selected γ-rays Used for Assay of ^{229}Th.

Radionuclide	Half-life	E_γ (keV)	I_γ (%)	Reference
^{229}Th	7932y	193.5 210.9	4.41 2.8	Nuclear Data Sheets Nuclear Data Sheets
^{228}Th	1.9y	216.0 238 (10.64h ^{212}Pb)	0.25 43.6	Nuclear Data Sheets Atomic Data and Nuclear Data Tables
^{227}Th	18.7d	210.6	1.25	Nuclear Data Sheets

3.4.1 Initial Assay Prior to Chemical Separation

One of the main goals of this project was to measure ^{229}Th ($t_{1/2}$ = 7932y) directly, but this can be very difficult due to very long half-life, relatively low intensity γ-rays, and presence of the undesirable bi-products created through the proton irradiation of natural thorium. The energies of two γ-rays of ^{229}Th of particular interest due to their high relative intensity at 193 keV and at 210 keV. ^{227}Th ($t_{1/2}$ = 18.68d) also emits a 210 keV γ-ray at a much higher intensity. Even though, due to its 18.7 d half-life, the majority of the original ^{227}Th created in the irradiation would have decayed, this radionuclide is also produced indirectly from the decay of ^{227}Ac ($t_{1/2}$ = 21.77y), as shown in Figure 2. Since it is not possible to chemically separate ^{227}Th from ^{229}Th, the only usable γ-ray for quantifying ^{229}Th activity is the 193 keV γ-ray. After irradiation, the 23 thorium foils were individually counted for a period of 15 hours each. One of the initial γ-ray spectra is shown in Figure 12. This sample was counted at 10 cm from the surface of the detector and the detector dead time was 3.03%. As can be seen in Figure 12, the photopeak of the 193 keV γ-ray

emitted directly from the decay of ^{229}Th is not visible over the Compton continuum of the higher energy γ-rays emitted from the higher activity byproducts such as ^{228}Th and its daughters. Consequently the activity of the ^{229}Th cannot be quantified without chemical purification.

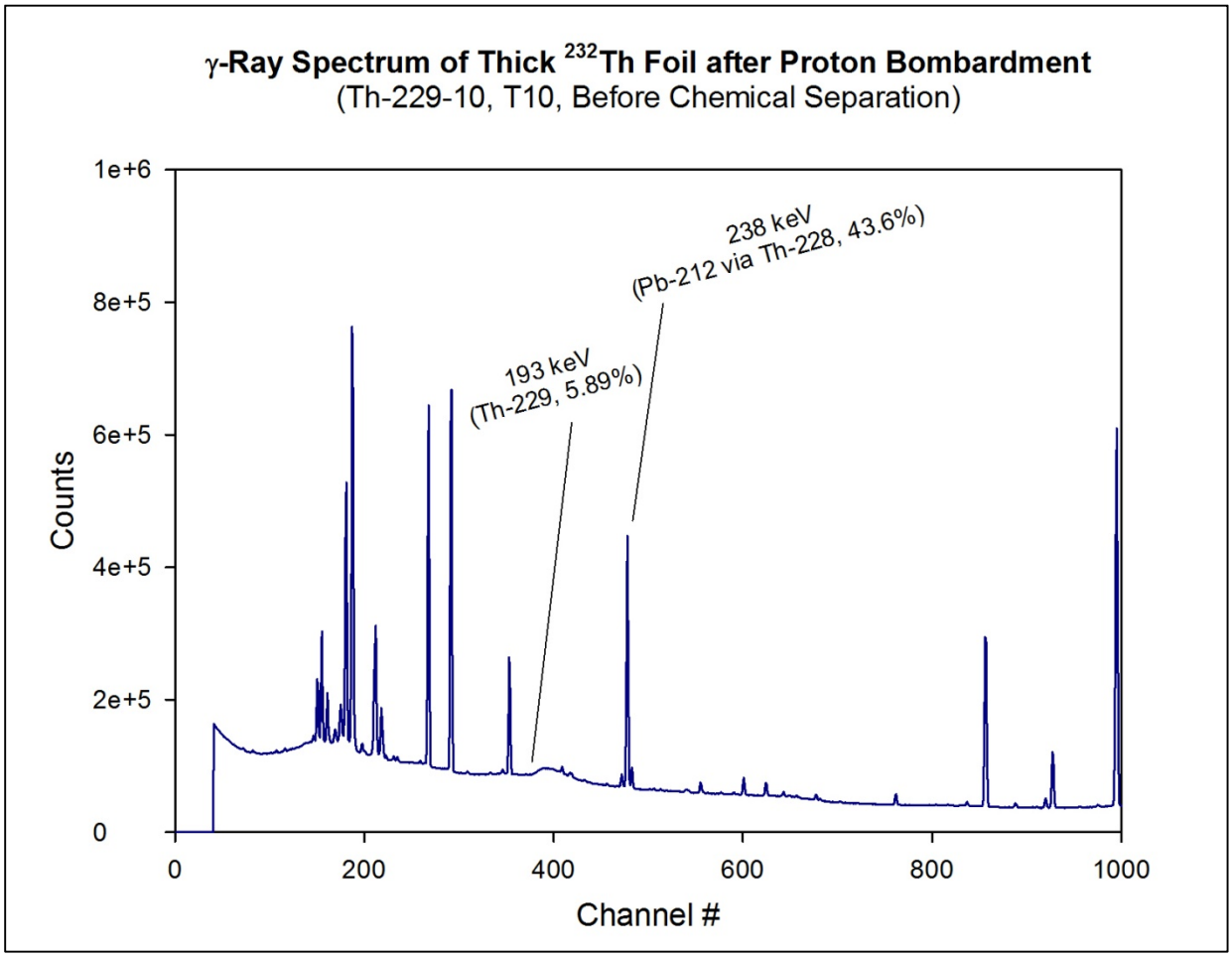

Figure 12. Spectrum of Foil Before Chemical Purification. It is important to note that the 193 keV photopeak is not visible.

3.4.2 Assay After Chemical Separation

After the final stage of chemical purification, each sample solution was counted using a counting algorithm that allowed for ten continuous five hour counts. This allowed enough

counting time for the 193 keV photopeak from ^{229}Th to become discernible above the background radiation, as can be seen in Figure 13. This sample was counted at 1 cm away from the surface of the detector and the detector dead time was < 1%. ^{212}Pb ($t_{1/2}$ = 10.64h), the daughter product of ^{228}Th ($t_{1/2}$ = 1.9y), grows back in very quickly and emits a very intense (43.6%) 238 keV γ-ray. Following the fourth or fifth 5 hour count, depending on activity of ^{228}Th in each sample, the 193 keV γ-ray is no longer visible above the Compton continuum created by the 238 keV γ-ray. This dramatic ingrowth can be seen by comparing Figure 13 and Figure 14. The first four counts of each sample are used to calculate the activity of ^{229}Th present. More detail about this calculation is provided in Chapter 4.

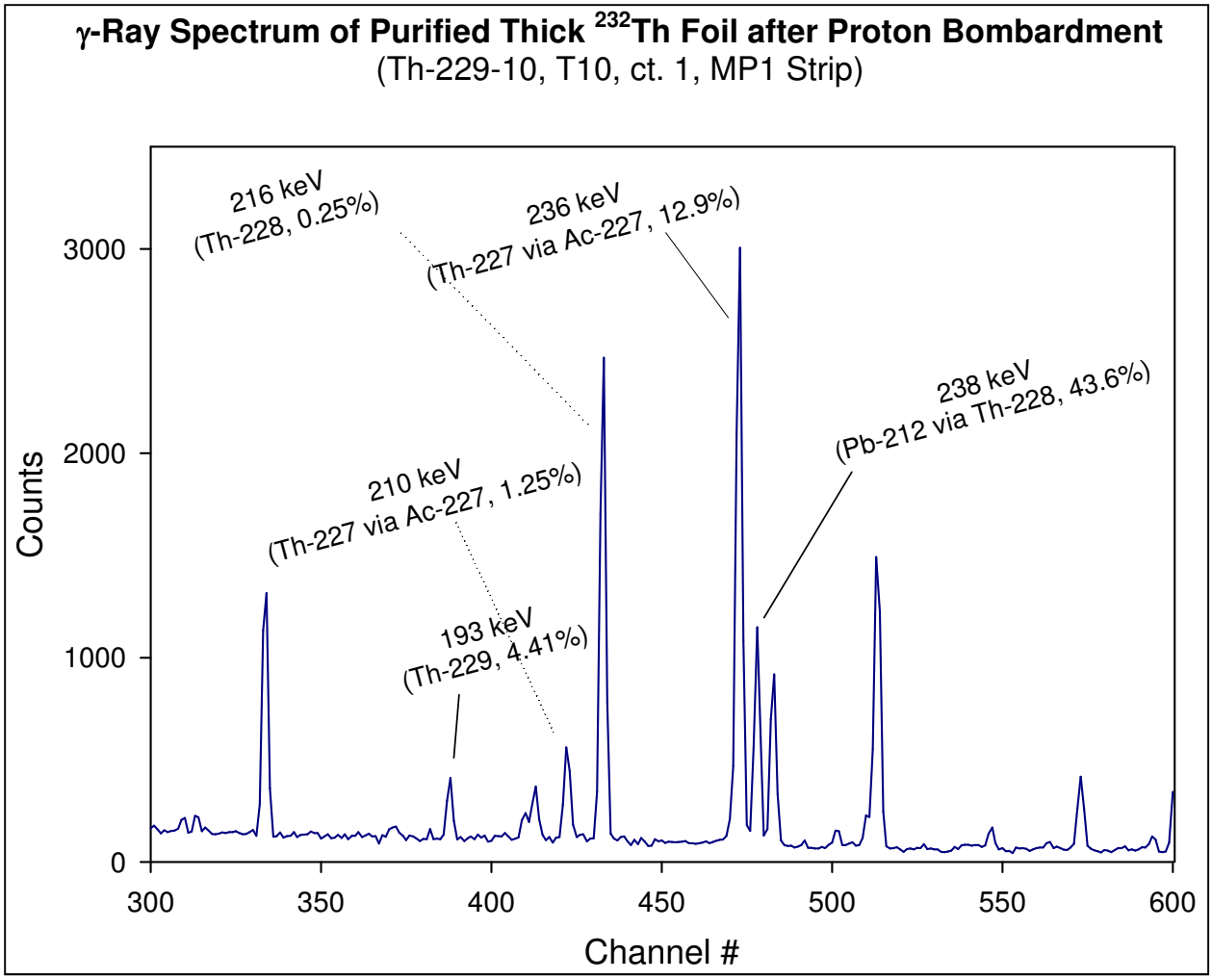

Figure 13. Spectrum of Foil After Chemical Purification but Before Ingrowth of ^{212}Pb. The sample was counted 1 cm from the surface of the detector with a dead time <1%.

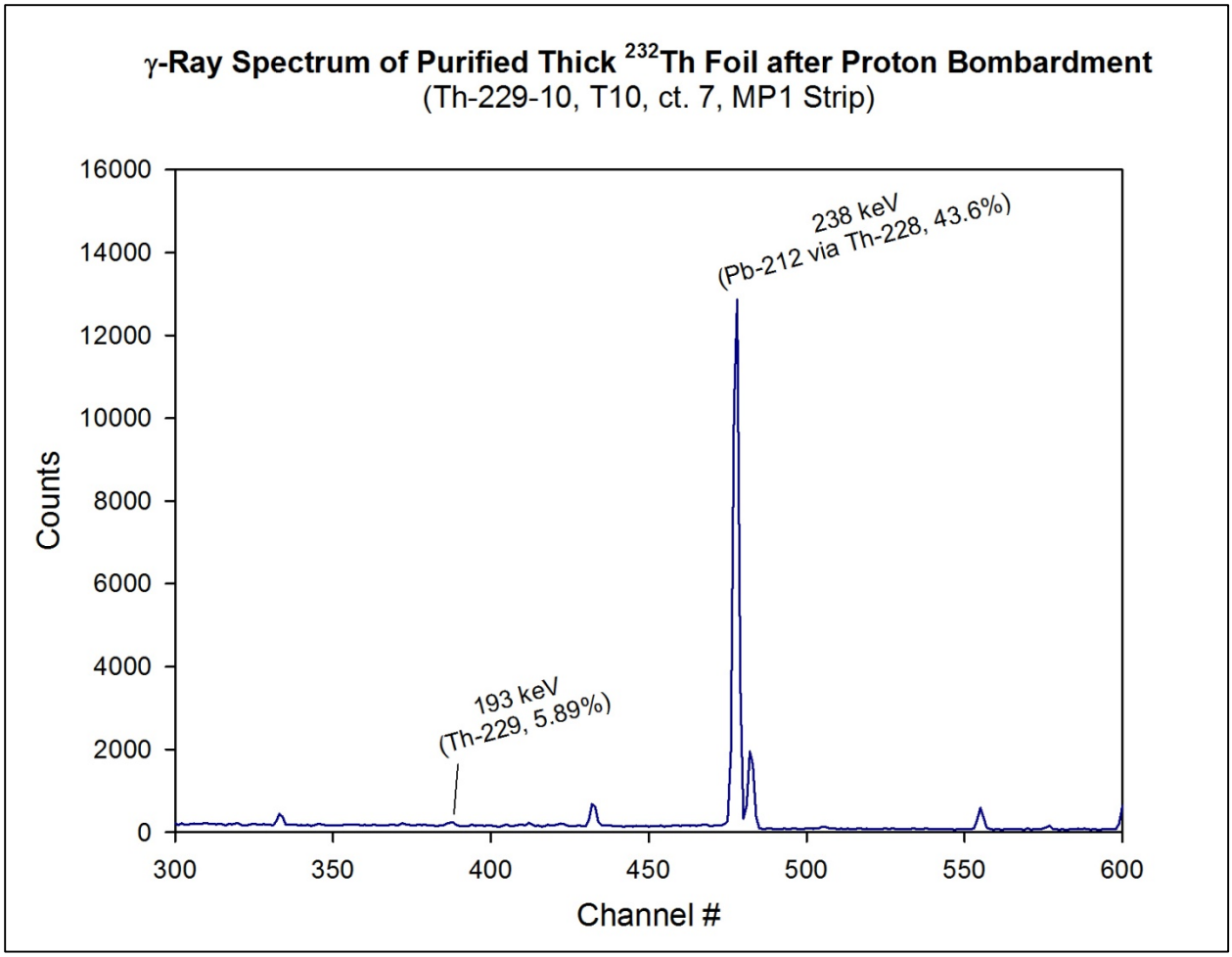

Figure 14. Spectrum of Foil After Chemical Purification After Ingrowth of ^{212}Pb.

3.4.3 Use of ^{228}Th as an Internal Radiotracer for Determination of Chemical Yield

In order to determine the chemical efficiency at which the thorium fraction was separated from the other products, ^{228}Th was used as a radiotracer. The ^{228}Th activity for each target before chemical separation was determined using the 238 keV γ-ray from its ^{212}Pb daughter. It can be assumed that the ^{212}Pb and the ^{228}Th were in secular equilibrium; i.e. the radioactivity of the ^{212}Pb and the ^{228}Th was equal in each sample. Secular equilibrium is possible because the longest-lived radionuclide in the ^{228}Th decay chain is ^{224}Ra ($t_{1/2}$ = 3.63d), which is much shorter-lived than the 1.9 year half-life ^{228}Th. A daughter radionuclide grows into secular equilibrium

with the parent radionuclide after about seven daughter half-lives. Since the foils were counted over 150 days after irradiation, both ^{224}Ra and ^{212}Pb were in secular equilibrium with ^{228}Th. Secular equilibrium is modeled by the following equation, where A_1 is daughter activity, A_0 is parent activity, λ_1 is the daughter decay constant, and t is time:

$$A_1 = A_0\left(1 - e^{-\lambda_1 t}\right)$$

After chemical separation, the secular equilibrium between ^{212}Pb and ^{228}Th is disrupted because all the lead and radium was removed from the target solution. However, the background radiation is reduced enough for the 216 keV γ-ray (0.25%) emitted directly by ^{228}Th to be observed. This photopeak can be seen in Figure 13. Activity of the ^{228}Th was calculated using this γ-ray, and the overall chemical efficiency was determined.

Chapter IV Results and Discussions

4.1 Activity Calculation

Following all of the chemical separations, the activity of each foil was calculated. Due to the long half-life of ^{229}Th ($t_{1/2}$ = 7932 ± 55 y) and the relatively low intensity of the 193 keV γ-ray (4.41%), a very low number of net counts were discernable above background for each sample. In many cases, the 193 keV photopeak was too small to be recognizable by the MCA software. In order to be able to measure the net counts of the 193 keV photopeak for each sample, a Microsoft Excel spreadsheet utilizing a simple algorithm was created. The first four continuous counts were summed to increase the peak area of the photopeak. No propagation of error is necessary for this step because it is assumed that the uncertainty in the gross number of counts per channel is zero. Additionally, it was assumed that the 193 keV photopeak was contained within four MCA channels and the energy calibration remained constant. The background underneath the 193 keV photopeak was determined by averaging the four channels before the photopeak and the four channels afterwards. The entire calculation of net peak area is shown below and Figure 15 further illustrates this method:

$$G = \sum_{n=5}^{8} n$$

$$B = \left(\frac{\sum_{n=1}^{4} n + \sum_{n=9}^{12} n}{8} \right) * 4$$

$$C = G - B$$

*Channel n=1 indicates the first channel for which the background average will be calculated (four channels before the first peak channel).

In the equations above, *G* is the gross number of counts under the photopeak, *B* is the number of background counts under the photopeak, and *C* is the net counts under the photopeak.

Propagation of error is necessary to determine the total uncertainty in the net peak area, σ_C; this calculation is shown below. In this case *s* is the sample standard deviation of the eight background channels and σ_s is the standard error of the eight background channels.

$$\sigma_G = \sqrt{G}$$

$$s = \sqrt{\frac{\sum_{i=1}^{N}(x_i - \bar{x}_e)^2}{N-1}}$$

$$\sigma_s = \frac{s}{\sqrt{N}}$$

$$\sigma_B = \sigma_s * 4$$

$$\sigma_C = \sqrt{{\sigma_G}^2 + {\sigma_B}^2}$$

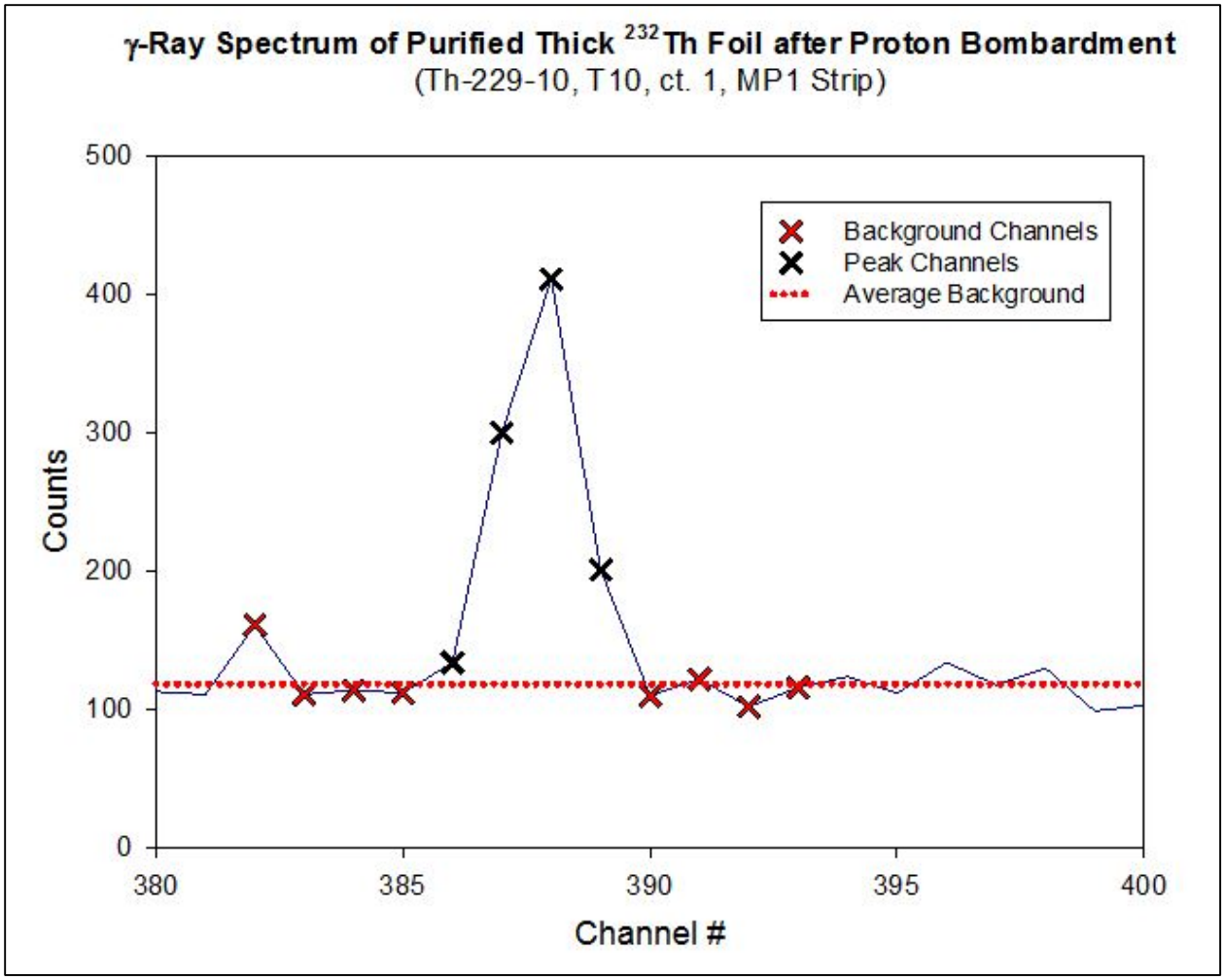

Figure 15. Depiction of method used to determine net peak area.

After determining the net peak area, activity at the time of count, A_{TOC}, was determined using the equation below where ε_{det} is detector efficiency, I_γ is the γ-ray intensity, and ε_{chem} is the overall chemical efficiency.

$$A_{TOC} = \frac{C}{\varepsilon_{det} * I_\gamma * \varepsilon_{chem}}$$

The uncertainty of A_{TOC} is calculated using the following equation, which propagates the uncertainty from the net peak area calculation, the uncertainty in the efficiency of the detector, and the uncertainty in the chemical efficiency.

$$\sigma_{A_{TOC}} = \sqrt{\left(\frac{\sigma_C}{C}\right)^2 + \left(\frac{\sigma_{\varepsilon_{det}}}{\varepsilon_{det}}\right)^2 + \left(\frac{\sigma_{\varepsilon_{chem}}}{\varepsilon_{chem}}\right)^2}$$

In order to calculate cross-section, it was necessary to convert activity at the time of count to activity at the end of bombardment. This conversion was completed using the following equation where λ is the decay constant of ^{229}Th and t is the time from the end of bombardment to the time of the assay.

$$A_{EOB} = \frac{A_{TOC}}{exp(-\lambda t)}$$

4.2 Cross Section Measurements

As described in Section 3.2.2, the irradiation of the thorium target foils was performed over five discontinuous periods. Therefore the decay during and between irradiation periods must be taken into account when determining the cross section of shorter-lived radionuclides. This correction was made to the ^{229}Th cross section even though the decay over these time periods was negligible due to its long half-life. In the equations below t_1, t_3, t_5, t_7, and t_9 correspond to intervals when the target was being irradiated. The variables t_2, t_4, t_6 and t_8 correspond to intervals when the target was not being irradiated but radioactive decay was occurring. To simplify these equations, the constant t' was used to combine all of these exponential terms.

$$t_a = [1 - exp(-\lambda t_1)] * exp(-\lambda t_2)$$

$$t_b = [1 - exp(-\lambda t_3)] * exp(-\lambda t_4)$$

$$t_c = [1 - exp(-\lambda t_5)] * exp(-\lambda t_6)$$

$$t_d = [1 - exp(-\lambda t_7)] * exp(-\lambda t_8)$$

$$t_e = 1 - exp(-\lambda t_9)$$

$$t' = t_a + t_b + t_c + t_d + t_e$$

Finally, the cross section of ^{229}Th was calculated for each sample using the equation below where N is the number of target (^{232}Th) atoms per cm^2 and φ is the proton current (protons/s). Current in nA is converted to φ by multiplying by the constant 6.24 x 10^9 protons/nC.

$$\sigma_{tot} = \frac{A_{EOB}}{N * t' * \varphi}$$

The uncertainty of the cross section measurement is entirely governed by the uncertainty in the net peak area due to the low count rate observed. The uncertainty in the chemical efficiency was much lower due to the higher count rate of γ-rays emitted by ^{228}Th and its daughter products. Uncertainty of the measured cross section is just the relative uncertainty of the net peak area multiplied by the value of the cross section as shown in the following equation.

$$uncertainty\ in\ \sigma_{tot} = \sigma_{tot} * \frac{\sigma_C}{C}$$

Table 5 shows the results of the effective thick target cross section measurements performed in this experiment. The 205 mb peak of the excitation function occurs at 26 MeV. A plot of the thick target excitation function is shown in Figure 16. Although 23 foils were irradiated, ^{229}Th was only detectable in 9 of the foils. This is to be expected as the cross section drops off at energies above 33 MeV and energies below 23 MeV. Background counts generated by ^{228}Th daughters also contributes to the inability to assay ^{229}Th outside the energy range shown in Table 5.

Table 5. ^{229}Th thick target cross sections.

Target Number	Energy (MeV)	Uncertainty (MeV)	Cross Section (mb)	Error (mb)
7	33.25	1.38E-02	98.10	18.45
8	32.14	1.19E-02	119.35	15.51
9	31.00	1.02E-02	143.45	13.81
10	29.83	1.20E-02	169.80	6.13
11	28.61	1.35E-02	139.57	9.90
12	27.37	1.42E-02	154.57	61.02
13	26.05	2.01E-02	204.58	17.59
14	24.70	1.82E-02	122.54	9.79
15	23.33	1.61E-02	90.89	9.79

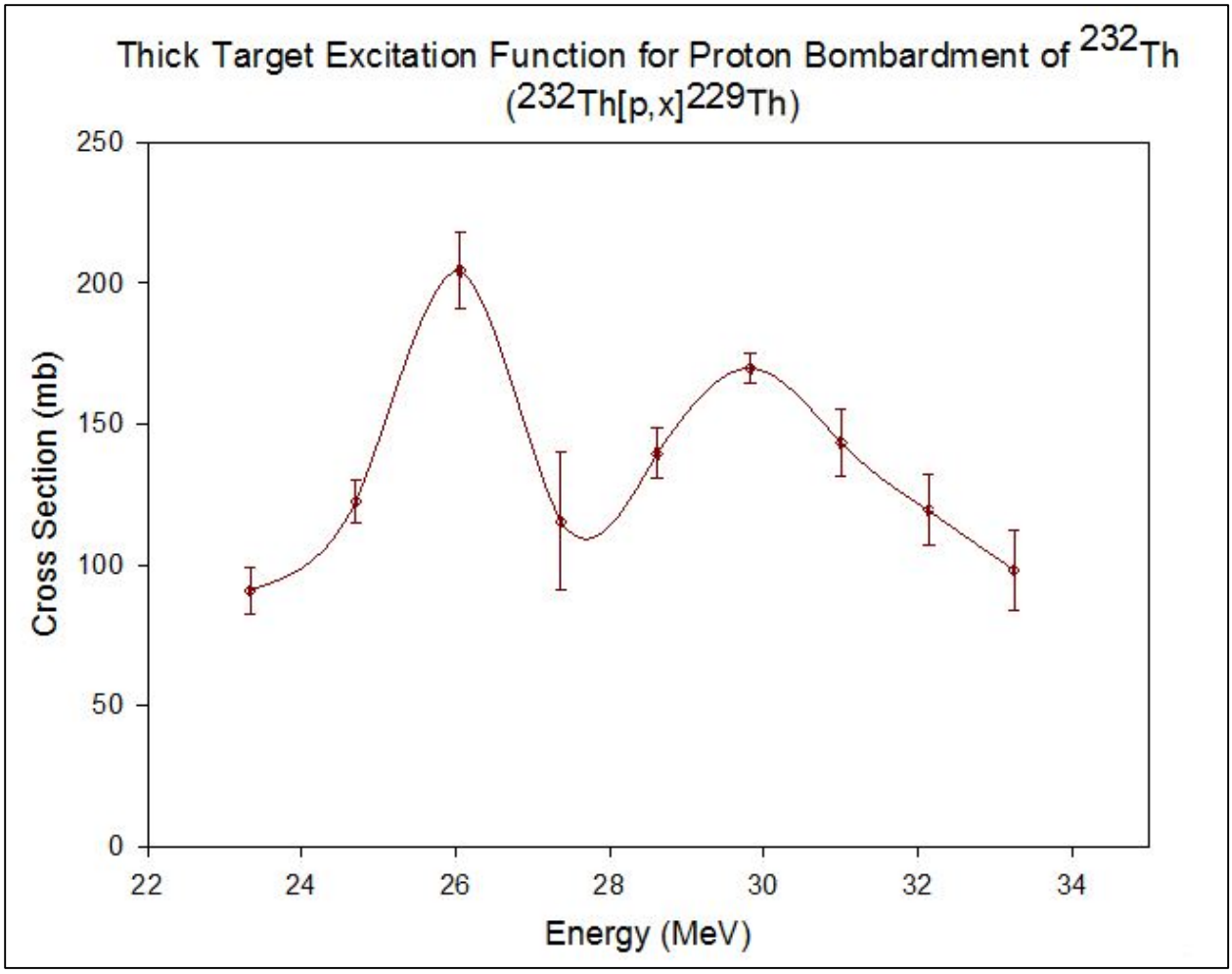

Figure 16. ^{229}Th thick target excitation function

As can be seen in Figure 16 above, the uncertainty for each of the cross section values is high. This is due to the low number of net counts collected from the 193 keV γ-ray of the long-lived ^{229}Th. The excitation function appears to have two peaks, which is unlike other measurements of excitation functions in this region as shown in Section 4.3. There are two possible explanations for the shape of this function. One explanation would be that the high uncertainty from the low count rate caused the function to dip. Another possible explanation could be the decline of the ^{232}Th[p, 4n]^{229}Pa excitation function and the subsequent rise of the ^{232}Th[p, α]^{229}Ac excitation function (Coulomb barrier at E_p = 27.9). Both of these reactions yield

^{229}Th after beta decay, which would affect the overall shape of the effective thick target excitation function.

4.3 Comparison of Similar Measurements

Cross sections from this experiment are compared with those measured in similar settings at ORNL using 10x thinner (0.0125 mm) natural thorium targets. The excitation functions shown in Figure 17 are the ^{232}Th[p, x]^{229}Th reaction from this thesis and the ^{232}Th[p, xn]$^{228, 229, 230, 232}$Pa reactions conducted at ORNL. For reference, the ^{232}Th[p, 3n]^{230}Pa excitation function from Morgenstern et. al is also included. The ^{232}Th[p, x]^{229}Th excitation function from this experiment has a similar magnitude as well as energy distribution to the ^{232}Th[p, 4n]^{229}Pa function.

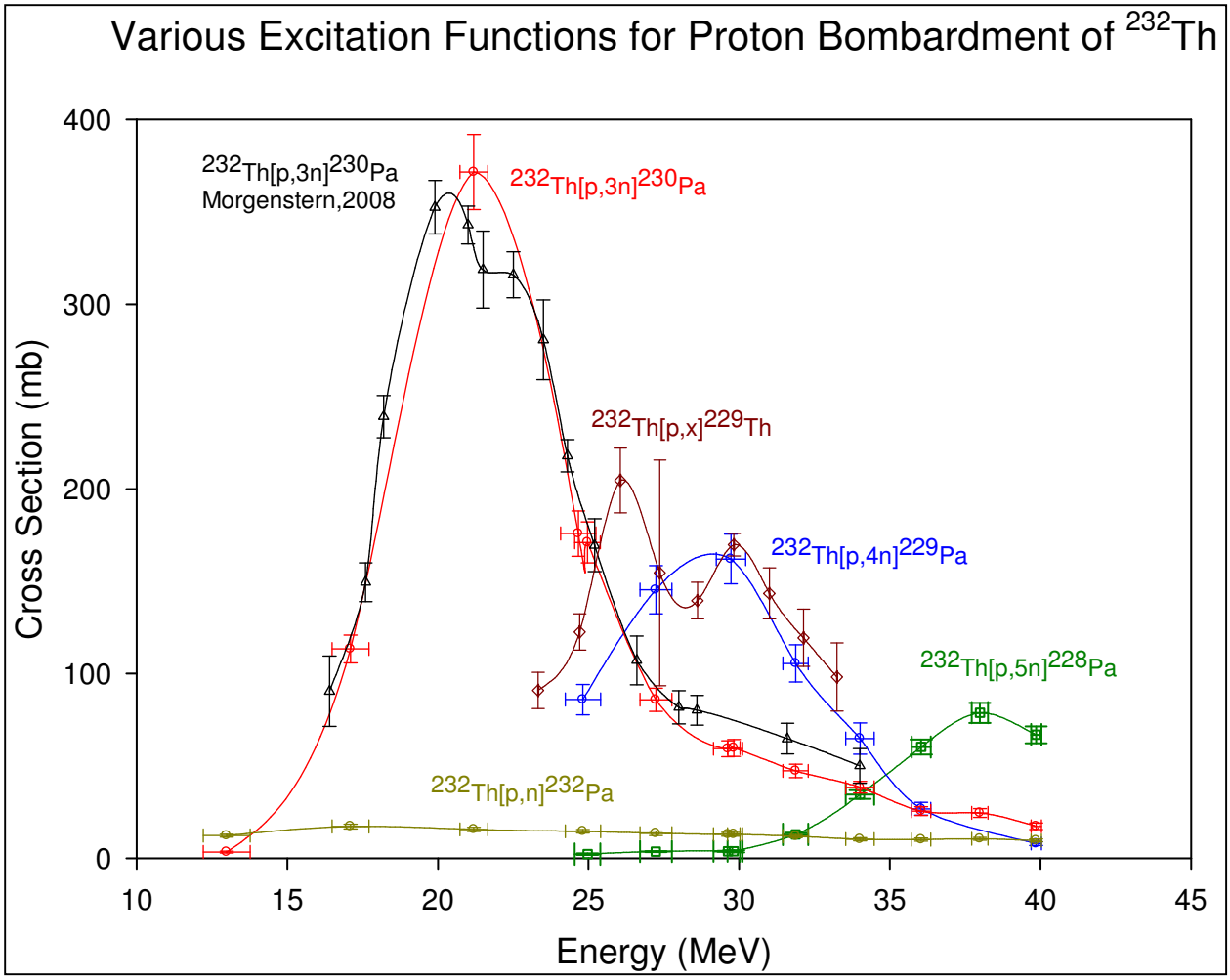

Figure 17. Comparison of ^{232}Th[p, x]^{229}Th to other cross section measurements of proton bombardment on a ^{232}Th target.

Chapter V Conclusions and Recommendations

The effective thick target cross section for the ^{232}Th[p, x]^{229}Th reaction was reported. Low count rates due to the long half life of ^{229}Th led to high values of cross section uncertainty; over 30% in one foil measurement. Bi-products such as ^{228}Th daughters add to the appreciable background, further complicating the γ-ray spectrum. If the separations were to be repeated 10 or more years later, over 96% of the ^{228}Th would have decayed away, allowing for much longer count times of ^{229}Th. This, in turn, would dramatically decrease the uncertainty of this measurement.

Although the ^{229}Th activity reported was low, the cross sections are large enough for significant production in another accelerator facility capable of currents in the100-300 μA range. Several such facilities exist, but lack the capability to house a thorium target for the several years necessary to obtain a sufficient supply (mCi quantities). It is important to note that the decay of ^{229}Th is not the only route through which ^{225}Ac can be produced. Currently research is being conducted in a joint effort by ORNL, Brookhaven National Lab, and Los Alamos National Lab to produce ^{225}Ac directly via high energy spallation (~200 MeV) of ^{232}Th. Initial results appear promising, with the expectation of producing Ci quantities of ^{225}Ac within the next several years.

List of References

1. Sgouros, G., "Alpha-Particles for Targeted Therapy," Advanced Drug Delivery Reviews 60, 1402 (2008).

2. Mulford, D.A.; Scheinberg, D.A.; Jurcic, J.G.; "The Promise of Targeted {Alpha}-Particle Therapy: Review," *J Nucl Med* 46, 199S (2005).

3. Allen, B.J.; Tian, A.; Rizvi, S.M.; Li, Y.; Ranson, M., "Preclinical Studies of Targeted Alpha Therapy for Breast Cancer Using ^{213}Bi-Labelled-Plasminogen Activator Inhibitor Type 2," *Br J Cancer* 88, 944 (2003).

4. Denardo, S.J., "Radioimmunodetection and Therapy of Breast Cancer: Review," *Semin Nucl Med* 35, 143 (2005).

5. "Alpha-Emitters for Medical Therapy." Conference. Denver, CO. May 30-31, 1996.

6. Jurcic, J.G.; Larson, S.M.; Sgouros, G.; McDevitt, M.R.; Finn, R.E.; Divgi, C.R.; Ballangrud, A.M.; Hamacher, K.A.; Ma, D.; Humm, J.L.; Brechbiel, M.W.; Molinet, R.; Scheinberg, D.A., "Targeted Alpha-Particle Immunotherapy for Myeloid Leukemia," *Blood* 100, 1233 (2002).

7. Sandmaier, B.M.; Bethge, W.A.; Wilbur, D.S.; Hamlin D.K.; Santos E.B.; Brechbiel M.W.; Fisher D.R.; Storb, R., "Bismuth-213-Labeled Anti-CD45 Radioimmunoconjugate to Condition Dogs for Nonmyeloablative Allogeneic Marrow Grafts," *Blood* 100, 318 (2002).

8. Stutchbury, T.K.; Al-ejeh, F.; Stillfried, G.E.; Croucher, D.R.; Andrews, J.; Irving, D.; Links, M.; Ranson, M., "Preclinical Evaluation of ^{213}Bi-Labeled Plasminogen Activator Inhibitor Type 2 in an Orthotopic Murine Xenogenic Model of Human Breast Carcinoma," *Mol Cancer Ther* 6, 203 (2007).

9. Kennel, S.J.; Boll, R.; Stabin, M.; Schuller, H.M.; Mirzadeh, S., "Radioimmunotherapy of Micrometastases in Lung with Vascular Targeted Bi-213," *Br. J. Cancer* 80, 175 (1999).

10. Dadachova, E.; Patel, M.C.; Toussi, S.; Apostolidis, C.; Morgenstern, A.; Brechbiel, M.W.; Gorny, M.K.; Aolla-Pazner, S.; Casadevall, A.; Goldstein, H., "Targeted Killing of Virally Infected Cells by Radiolabeled Antibodies to Viral Proteins," *PLoS Medicine* 3, 3427 (2006).

11. Couturier, O.; Supiot, S.; Degraef-Mougin, M.; Faivre-Chauvet, A.; Carlier, T.; Chatal, J.F.; Davodeau, F.; Cherel, M., "Cancer Radioimmunotherapy with Alpha-emitter Nuclides: Review," *Eur J. Nucl. Med. Mol. Imaging* 32, 601 (2005).

12. Mirzadeh, S., "Generator-produced Alpha-emitters," *Applied Radiat. Isot*. 49, 345 (1998).

13. Miederer, M.; Scheinberg, D.A.; McDevitt, M.R., "Realizing the Potential of the Actinium-225 Radionuclide Generator in Targeted Alpha Particle Therapy Applications," *Advanced Drug Delivery Reviews* 60, 1371 (2008).

14. McDevitt, M.R.; Ma, D;, Simon, J.; Frank, R.K.; Scheinberg, D.A., "Design and Synthesis of ^{225}Ac Radioimmunopharmaceuticals", *Applied Radiation and Isotopes* 57, 841 (2002).

15. Cherel, M.; Davodeau, F.; Kraeber-Bodere, F; Chatal, J.F., "Current Status and Perspectives in Alpha Radioimmunotherapy: Review," *Q J Nucl Med Mol Imaging* 50, 3222 (2006).

16. Brechbiel, M.W., "Targeted Alpha-therapy: Past, Present, Future?: Review," *Dalton Trans* 21, 4918 (2007).

17. Boll, R.A.; Malkemus, D.; Mirzadeh, S., "Production of Actinium-225 for Alpha Particle Mediated Radioimmunotherapy," *Applied Radiation and Isotopes* 62, 667 (2005).

18. Boll, R.A.; Garland M.A.; Mirzadeh, S.; "Reactor Production of Th-229 at the ORNL High Flux Isotope Reactor," *Trans. Am. Nucl. Soc.* 98, 814 (2008).

19. Morgenstern, A.; Apostolidis, C.; Bruchertseifer, F.; Capote, R.; Gouder, T.; Simonelli, F., "Cross-sections for the Reaction Th-232(p,3n)Pa-230 for Production of U-230 for Targeted Alpha Therapy," *Applied Radiation and Isotopes* 66, 1275 (2008).

20. Turner, J. E. (2007). Atoms, radiation, and radiation protection (3rd completely rev. and enl. ed.). Weinheim: Wiley-VCH.

21. Meigs, M.J.; Haynes, D.L.; Jones, C.M.; Juras, R.C., "Development of the HRIBF 25-MV Tandem Accelerator as a RIB Accelerator," *Nucl. Instr. and Meth. A* 382, 51 (1996).

22. Ziegler, J.F.; Biersack, J.P.; Littmark, U., "The Stopping and Range of Ions in Solids," Pergamon Press, New York (1985) and SRIM website, www.srim.org (2009).

23. Engle, J.W.; Mashnik, S.G.; Weidner, J.W.; Wolfsberg, L.E.; Fassbender, M.E.; Jackman, K.; Couture, A.; Bitteker, L.J.; Ullmann, J.L.; Gulley, M.S.; Pillai, C.; John, K.D.; Birnbaum, E.R.; Nortier, F.M., "Cross sections from proton irradiation of thorium at 800 MeV," *Phys. Rev. C. 88 (2013)*

24. National Institute of Standards and Technology Physical Measurement Laboratory "http://www.nist.gov/pml/data/star/index.cfm." Accessed June 2010.

25. Ahmad, I; Gindler, J.E.; Friedman, A.M.; Chasman, R.R.; Ishii, T., "Level Structure of ^{225}Ac," *Nucl. Phys. A* 472, 285 (1987).

26. Jost, C.U.; Griswold, J.R.; Bruffey, S.H.; Mirzadeh, S.; Stracener, D.W.; Williams, C.L.,"Measurement of cross sections for the ^{232}Th (p, 4n) ^{229}Pa reaction at low proton energies," *AIP Conference Proceedings*1525, 520 (2013).

Vita

Justin Griswold was born in Knoxville, Tennessee on June 11, 1990. He graduated from Farragut High School in Knoxville in 2008. He then attended the University of Tennessee and received his Bachelor of Science in Nuclear Engineering in 2012. He continued his education at the University of Tennessee where he will receive his Master of Science in Nuclear Engineering. He continues to pursue a doctorate in Nuclear Engineering at the University of Tennessee.